nature sustainability

Article

https://doi.org/10.1038/s41893-026-01887-8

Sustainable all-silk textiles for personal thermal management

Received: 17 October 2024

Accepted: 30 May 2026

Published online: 22 June 2026

Check for updates

Xun-En Wu[1,5], Yida Wang[1,5], Shuo Li[1], Yong Zhang[1], Haojie Lu[1], Lin Zhu[2], Muqiang Jian[3], Meihui Jiang[4], Mengjia Zhu[1], Mei Zou[1], Huarun Liang[1], Yaoyao Zhou[1], Peng Bi[1], Xiaoping Liang[1], Renchuan You[2], Wenshuai Chen[4] ✉ & Yingying Zhang[1] ✉

Hierarchically structured synthetic textiles incorporating pores or nanoparticles have demonstrated considerable promise for daytime radiative cooling. However, their widespread adoption is constrained by substantial risks to environmental and human health, including microplastic shedding and nanoparticle toxicity. Here we report an all-silk nanotextile (SilkNT) that delivers high-performance radiative cooling while remaining entirely free of synthetic polymers and toxic additives. Fabricated by wrapping silk nanofibres around silk yarns using a Fermat-spiral twisting technique, SilkNT leverages hierarchical architecture and inherent optical properties of the material to achieve a remarkable solar reflectance of 94.8% and a reduced UV absorption of 8.19%. Under practical applications, skin covered by SilkNT exhibits a 4.3 °C lower temperature than that covered with conventional silk fabric. Comprehensive experimental characterizations and life cycle assessment confirm the material's exceptional biodegradability, recyclability, biocompatibility and reduced environmental impact. This work establishes a sustainable engineering paradigm for next-generation high-performance cooling textiles with a minimal ecological footprint.

Rising global temperatures have created an urgent demand for textiles that alleviate daytime heat stress[1]. Synthetic textiles, constituting 64% of global textile production[2], are widely used for enhancing skin comfort owing to their versatile designability and excellent processability[3,4]. Extensive research has been conducted on their potential for daytime radiative cooling. A variety of materials, such as polytetrafluoroethylene[5–8], polyvinylidene fluoride[6,9], poly(vinylidene fluoride-co-hexafluoropropylene) (PVDF-HFP)[10], polyethylene oxide[11,12], polyformaldehyde[8,13], styrene ethylene butylene styrene[14], thermoplastic polyurethane[15,16], polydimethylsiloxane (PDMS)[17] and polyethylene (PE)[18], have been explored for the creation of daytime radiative cooling textiles, through nanoparticle modification (aluminium oxide[14,19], zinc oxide[20], titanium oxide[5], silicon nitride[15] and so on) or sophisticated structural design approaches[7,8,18]. However, these composites raise concerns about the potential microplastic pollution and toxic nanoparticle detachment during everyday use, posing a risk to both the environment and human health[3,21–26]. Consequently, there is a pressing need to develop sustainable cooling textiles that avoid such hazards.

Silk is a fully biodegradable material without microplastic pollution concerns[27,28]. Its potential for daytime radiative cooling[29,30] surpasses that of other natural or bio-derived materials, such as cotton[31], bastose (mainly composed of cellulose)[32] and polylactic acid[5]. Silk exhibits a higher refractive index (1.51 in the wavelength range of 0.400–1.05 μm) than that of polylactic acid (1.48 in the wavelength

[1]Key Laboratory of Organic Optoelectronics and Molecular Engineering of the Ministry of Education, Department of Chemistry, Tsinghua University, Beijing, People's Republic of China. [2]State Key Laboratory of New Textile Materials and Advanced Processing Technologies, Wuhan Textile University, Wuhan, People's Republic of China. [3]Beijing Graphene Institute, Beijing, People's Republic of China. [4]Key Laboratory of Bio-based Material Science and Technology of Ministry of Education, Northeast Forestry University, Harbin, People's Republic of China. [5]These authors contributed equally: Xun-En Wu, Yida Wang. ✉e-mail: chenwenshuai@nefu.edu.cn; yingyingzhang@tsinghua.edu.cn

range of 0.405–0.635 μm (ref. 33)) and cellulose (1.47 in the wavelength range of 0.437–1.05 μm (ref. 34)). At the same time, it has favourable infrared emittance[29], intrinsic ultraviolet (UV) photoluminescence and skin compatibility. Previous studies have shown that the intrinsic nanostructures of natural silk, including its nanofibrillar architecture[29] and randomly distributed nanopores[30], can confine light propagation through transverse Anderson localization, contributing to strong light scattering and enhanced solar reflectance. However, natural silk fibres, with diameter around 10 μm, have low efficiency for solar reflectance due to a mismatch with the wavelength range of sunlight. Moreover, the intensive UV absorption of natural silk leads to an undesirable energy gain from the radiation. Therefore, pure natural silk, although it possesses inherent biodegradability and favourable optical properties for radiative cooling, has inefficient solar reflectance and strong UV absorption, limiting its performance for subambient daytime radiative cooling. To fully unlock the potential of silk for effective daytime radiative cooling, it is essential to enhance its solar reflectance capabilities.

Several strategies have been developed to enhance the solar reflectance of materials. One approach is to modify yarns or textiles with nanoparticles, either through coating (nanoparticle@yarn) or embedding (nanoparticle/yarn). According to the Mie theory, hierarchical structures can notably improve solar scattering efficiencies over pristine ones[35]. However, these methods also pose risks of toxic nanoparticles or microplastic release. In the case of nanoparticle@yarn[14,19], exposed nanoparticles may detach during use, causing tactile discomfort and potential health hazards[26]. For nanoparticle/yarns, the outer layer encapsulating the nanoparticles may diminish light scattering efficiency, often requiring an additional petroleum-based polymer coating[5,7,17], which in turn elevates the potential for microplastic release. Another strategy is to create porous structures directly on yarns, although the materials used are typically synthetic[18,36], again contributing to microplastic pollution. Beyond woven textiles, non-woven nanofibre textiles have also been studied for daytime radiative cooling[7,8,11,37,38], yet their limited mechanical strength[11,37,38] often requires reinforcement with petroleum-based polymers, further increasing microplastic release risks[7,8]. The release of microplastics and toxic nanoparticles not only exacerbates environmental pollution but also poses direct risks to human health. Therefore, the development of microplastic- and toxic nanoparticle-free sustainable textiles is highly desired to achieve environmentally and biologically friendly daytime radiative cooling.

In this study, we show an all-silk nanotextile (SilkNT) fabricated via a Fermat-spiral twisting technique that wraps silk nanofibres around commercial silk yarns. This hierarchical core-shell architecture—free from synthetic polymers and toxic additives—leverages the inherent optical properties of silk to achieve a solar reflectance of 94.8% and an infrared emittance of 96.3% within the atmospheric transparency window, while simultaneously reducing UV absorption from 43.6% to 8.19%. Under peak solar radiation (839.1 W m^{-2}), SilkNT maintains a surface temperature 18.4 °C lower than bare simulated skin and at least 8.0 °C lower than conventional silk, acetate and cotton fabrics. When applied to human skin, SilkNT provides a 4.3 °C cooling effect compared with pristine silk. Beyond its thermal performance, SilkNT maintains tactile comfort, breathability and mechanical robustness while inherently eliminating the risk of microplastic or nanoparticle release. A life cycle assessment (LCA) further confirms that this all-silk construction substantially reduces environmental impact compared with existing nanoparticle-modified cooling textiles, establishing a sustainable paradigm for personal thermal management.

Results

Fabrication of SilkNT

Figure 1a illustrates the preparation process of SilkNT through Fermat-spiral twisting of silk nanofibres on commercial silk yarns. Conventional silk yarns are composed of natural silk fibres that have diameters of approximately 10 μm (Supplementary Fig. 1). According to the Mie scattering theory, these microscale fibres are not efficient as scattering media for solar reflection[35]. To address this, we wrapped silk nanofibres at a certain twisting angle (α) around the conventional silk yarns through a Fermat-spiral twisting technique (details shown in Methods), obtaining silk nanoyarns (SilkNYs). The nanofibres form a robust network layer arranged in a Fermat-spiral pattern[39] (Supplementary Figs. 2 and 3 and Supplementary Video 1). X-ray computed microtomography was employed to investigate the internal structure of SilkNYs, revealing that the silk nanofibres uniformly encase the silk yarns (Supplementary Fig. 4 and Supplementary Video 2). The SilkNYs are subsequently woven into SilkNT that exhibits a hierarchical micro-nanostructured surface (Supplementary Figs. 5 and 6).

Optical properties of SilkNT

The intrinsic optical properties of silk and the structural design co-contribute to the excellent optical performance of the SilkNT, enabling solar reflection and mid-infrared emission. We studied the optical characteristics of regenerated silk materials. The refractive index (n) and extinction coefficient (k) of the silk show that it has rare absorption in solar wavelength (Fig. 1b). According to Fresnel's law of reflection, the high refractive index observed in regenerated silk (1.51 in the wavelength range of 0.400–1.05 μm) contributes to the enhancement of interfacial reflection. The peak of the curve in the infrared range verifies the considerable infrared absorption. This proves that the regenerated silk has the potential for high infrared emittance according to Kirchhoff's laws of radiation[40]. Similarly, the attenuated total reflection Fourier-transform infrared spectrum of the regenerated silk film also confirms its strong infrared absorption (Supplementary Fig. 7).

The inherent fluorescence of the regenerated silk also contributes to rejecting solar energy input. Specifically, the absorbed solar light in the UV range (300–360 nm) can be transformed into visible light emission (Fig. 1c). The emissive process leads to a reduced heat gain process due to the additional photon-to-photon conversion[41,42]. The emission peak at 406 nm, which is excited by 330 nm UV light, confirms the intrinsic fluorescence properties of silk (Fig. 1d). We further characterized the absolute quantum yield under specific excitation wavelengths and calculated its energy conversion efficiency (Supplementary Fig. 8). By considering the energy distribution in UV radiation, we demonstrated that regenerated silk converts 2.6% of the absorbed energy in the UV range into fluorescence (Supplementary Fig. 9). Consequently, the intrinsic UV fluorescence of the regenerated silk is a non-negligible factor contributing to the heat dissipation of the SilkNT.

Besides, we also evaluated the influence of the nanofibre diameter on the solar reflection performance. We first conducted the numerical simulation on the electric field distribution of a single regenerated silk nanofibre under electromagnetic wave radiation (Fig. 1e, Supplementary Fig. 10 and Supplementary Note 1). The result shows that the incident wave can be strongly scattered to the surroundings. We also calculated the scattering efficiency of the regenerated silk nanofibres (Fig. 1f and Supplementary Fig. 11). This indicates that the nanofibres can efficiently scatter solar light when their diameters are close to the solar wavelength. The results are consistent with the Mie scattering theory. Accordingly, we optimized the diameters of regenerated silk nanofibres. Figure 1g shows the size distribution of the regenerated silk nanofibres. A Gauss distribution of diameter size was selected to coincide with the band of the standard solar spectra. We further evaluated the electric field distribution of the dense nanofibre layer under irradiation (Fig. 1h, Supplementary Fig. 12 and Supplementary Note 1). The results show that the nanofibres can effectively prevent light penetration, especially in the intensive solar band. The obtained SilkNT achieves both high solar reflectance of approximately 94.8% (in the range from 0.3 to 2.5 μm) and high infrared emittance of 96.3% in the atmospheric transparent window (Fig. 1i

https://doi.org/10.1038/s41893-026-01887-8

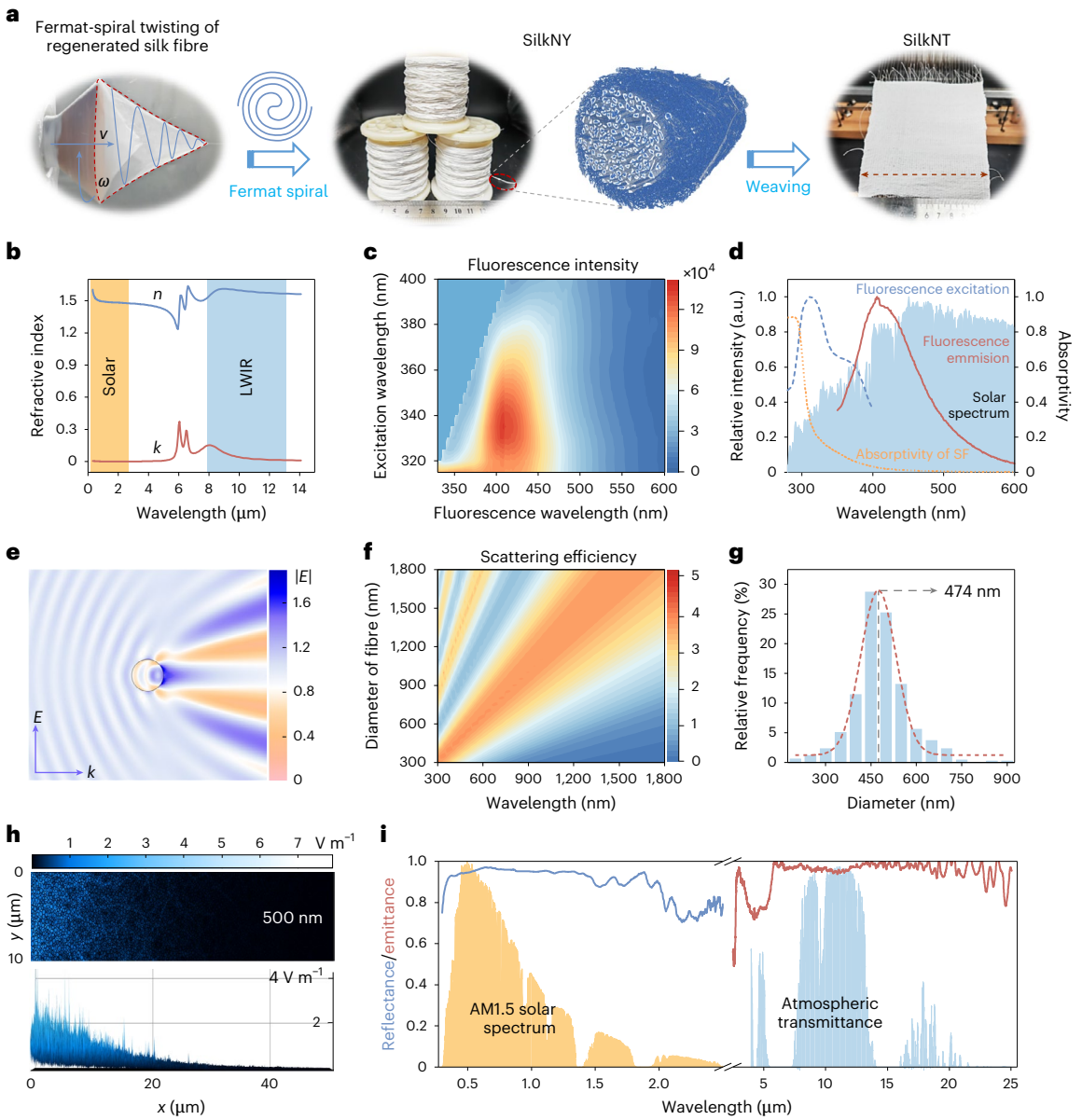


Fig. 1 | Preparation and optical properties of SilkNT. a, A schematic illustration showing the Fermat-spiral twisting preparation process of SilkNT. The dashed red double-headed arrow indicates the sample width of 12 cm. **b**, The complex refractive index ($n - ik$) of the regenerated silk. LWIR, long-wavelength infrared. **c**, Fluorescence mapping of a cast-regenerated silk fibroin (SF) film. **d**, Absorption, fluorescence excitation and emission spectra of the cast-regenerated SF film overlaid with the normalized solar spectrum. **e**, Simulated electric field distribution of a 500-nm regenerated silk nanofibre under 500-nm light radiation (cross-sectional view). The polarization direction of the electric field is perpendicular to the fibre axis. **f**, Simulation mapping of the scattering efficiency conducted in regenerated silk nanofibres. The polarization direction of the electric field is perpendicular to the fibre axis. **g**, Size distribution of regenerated silk nanofibres on the surface of the SilkNY. Diameter distribution was calculated from 516 fibres. **h**, Simulated electric field distribution of dense nanofibres with diameters of 457 nm ± 90 nm under 500-nm light radiation. **i**, Spectral reflectance of the SilkNT with normalized American Society for Testing and Materials (ASTM) G173 solar global spectrum and the atmospheric transparency window plotted for reference. The atmospheric transmittance $T_{atm}(\lambda, \theta = 0°)$ at 4–25 μm was calculated using ATRAN, a web-based software provided by SOFIA Science Center[7].

and Supplementary Note 2 for calculation details), exhibiting great potential for daytime radiative cooling.

The hierarchical structure on the surface of SilkNT boosts reflectance across the entire solar spectrum while maintaining the high infrared emittance inherent to natural silk (Supplementary Fig. 13). The solar reflectance of SilkNT reaches 94.8%, representing a substantial improvement over the 65.5% reflectance of conventional commercial silk textiles (Supplementary Fig. 14). In addition, the UV band absorbance of SilkNT is reduced to 8.19%, which is much lower than that of commercial silk textiles (43.6%). For comparison, we also modified pristine silk yarns using a typical synthetic polymer (PVDF-HFP)[43–47]. The solar reflectance of the PVDF-HFP-modified textiles is lower than 90% (Supplementary Figs. 15 and 16), highlighting the superior performance of SilkNT.

Previously reported daytime radiative cooling textiles mainly include natural materials with[19,48] or without[37] nanoparticles, synthetic materials with nanoparticles[12,14–16,49,50] and hybrid synthetic–natural materials with[5] or without[51] nanoparticles. By contrast, SilkNT is composed exclusively of silk, eliminating concerns about microplastic release or toxic nanoparticles. We simulated the cooling power demand using a one-dimensional steady-state heat transfer model to show the advantages of the SilkNT compared with previous work (Supplementary

https://doi.org/10.1038/s41893-026-01887-8

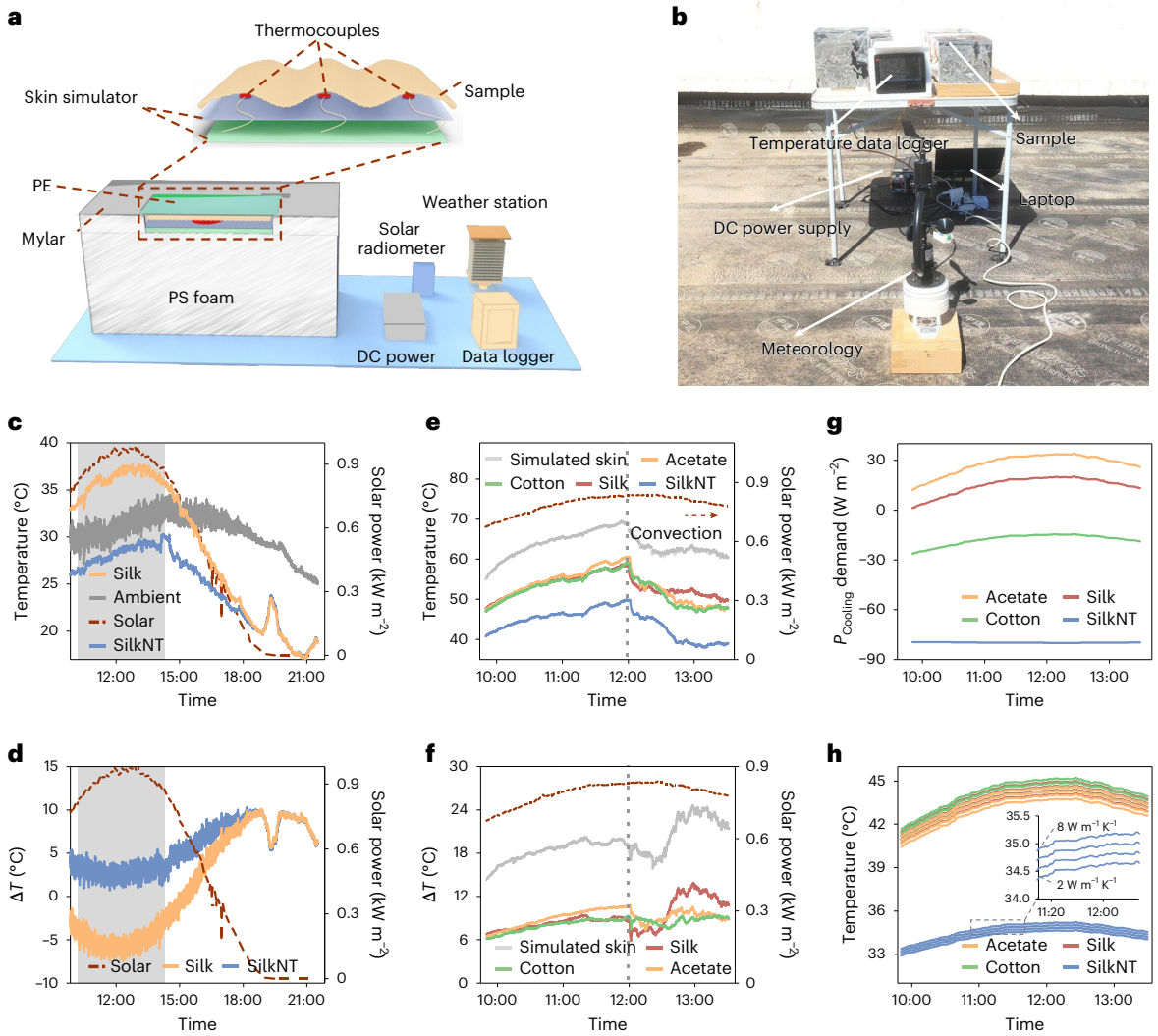


Fig. 2 | Daytime radiative cooling performance of SilkNT. a,**b**, A schematic (**a**) and optical image (**b**) of the thermal monitoring system used to characterize daytime radiative cooling performance. PS, polystyrene; DC, direct current. **c**, Evolution of temperature with time of simulated skin covered by the SilkNT and a commercial silk textile without additional heating (Beijing, 18 May 2023). The grey area shows the time period 10:00–14:00. **d**, The temperature difference in contrast to the ambient temperature ($\Delta T = T_{ambient} - T_{sample}$) of simulated skin covered by the SilkNT (average 2.9 °C at 10:00–14:00) and a commercial silk textile (average 5.1 °C at 10:00–14:00) without additional electrical heating (Beijing, 18 May 2023). **e**, Temperature of simulated skin in bare and covered by different textiles with additional electrical heating to simulate real human skin (Beijing, 23 June 2022). **f**, Temperature difference ($\Delta T = T_{commercial\ textile/bare\ skin} - T_{SilkNT}$) of simulated skin in bare and covered by different textiles with additional electrical heating (Beijing, 23 June 2022), compared with that covered by the SilkNT. **g**, Calculated cooling power demands of the simulated skin covered by SilkNT, silk, cotton and acetate to maintain a comfortable skin temperature of 34 °C (convective coefficients of 2 W m^{-1} K^{-1}). **h**, The calculated outer-surface temperatures of the SilkNT, silk, cotton and acetate at different convective coefficients (2, 4, 6 and 8 W m^{-1} K^{-1}).

Note 3, Supplementary Fig. 17 and Supplementary Table 1). The cooling performance of SilkNT is comparable to that of the most advanced daytime radiative cooling textiles reported so far (Supplementary Fig. 18).

Daytime radiative cooling performance of SilkNT

We evaluated the outdoor daytime radiative cooling performance of the SilkNT using a custom-designed apparatus (Fig. 2a). This set up features a simulated skin component (bottom), thermocouples (middle) for temperature measurement and the test textiles (top), all arranged within the projection area. The simulated skin was made with a PDMS-coated copper plate with paint and a polyimide flexible heater, which has similar optical properties to real skin[20] (Supplementary Figs. 19 and 20).

We placed the sample (that is, simulated skin covered by thermocouples and textiles) in a polystyrene foam groove with extremely low thermal conductivity and followed by encapsulating it with PE film to reduce the influence of heat conduction and convection (Fig. 2a,b and Supplementary Figs. 21 and 22). We recorded the temperature evolution of the simulated skin covered by a commercial silk textile and our SilkNT (Fig. 2c,d). The results show that the SilkNT maintained an average temperature difference of 2.9 °C from the surrounding air (solar power testing data, 10:00–14:00, 921.0 W m^{-2}; solar power referenced data, 10:00–14:00, 893.0 W m^{-2} from NASA; Supplementary Fig. 23). By contrast, the commercial silk textile was 5.1 °C higher than the ambient temperature under the same conditions, indicating no cooling effect. We also compared the daytime radiative cooling performance of the SilkNT with that of various commercial textiles of similar thicknesses (Supplementary Figs. 24–27). The solar reflectance and infrared emittance of commercial textiles were all lower than those of SilkNT (Supplementary Figs. 28 and 29), confirming the superior optical properties of SilkNT for daytime radiative cooling. It is noted that the selected commercial textiles with different woven structures

(Supplementary Fig. 30) have higher gram per square metre and fill factor (Supplementary Note 4) than the SilkNT. During the tests, the simulated skin was powered at a constant voltage (1.71 V, 100 W m^{-2}) to simulate the thermal conditions of real skin (Supplementary Fig. 31) and the testing box was unsealed to replicate real-world environmental conditions. The results (Fig. 2e,f) indicate that the SilkNT has outstanding cooling performance compared with other textiles. Average temperature differences of 8.3 °C, 9.0 °C, 8.0 °C and 18.4 °C were achieved by SilkNT compared with silk, acetate, cotton and with no cover, respectively, under the same environmental conditions (9:50–12:00) (Supplementary Fig. 32). Even in convective conditions (Supplementary Fig. 33), the temperature differences remained substantial. The results prove that the SilkNT has highly efficient daytime radiative cooling performance.

In addition, we validated the outstanding cooling performance of SilkNT through theoretical simulations (Supplementary Note 3, Supplementary Fig. 17 and Supplementary Table 2). First, the additional cooling power of the various textiles that are required to maintain the skin surface temperature of 34 °C (that is, the normal skin temperature) under external heating power (that is, simulated solar radiative heating) was calculated. The results show that both cotton textiles and SilkNT can stably maintain the skin surface temperature at 34 °C without additional thermal energy input (Fig. 2g). By contrast, the skin covered by silk and acetate textiles requires additional cooling power, indicating that the SilkNT has a superior ability to reject thermal energy. Even with varying convective coefficients (Supplementary Fig. 34), SilkNT consistently shows higher cooling power. Moreover, the surface temperature of the SilkNT is the lowest in comparison to the other three textiles (Fig. 2h). These results affirm that the SilkNT has superior cooling performance.

Suitability of SilkNT for wearing

The Fermat spinning process preserves the inherent mechanical strength of the original silk yarns (Fig. 3a) to ensure the durability for daily wear. The wettability of the SilkNT was evaluated by dispensing water droplets on its surface and tracking their behaviour over time. Upon initial contact, the droplet forms an angle of 128° ± 6° (Supplementary Fig. 35), indicating the resistance of SilkNT to immediate water penetration. Then, the droplets penetrated into the textile within 1 min (Supplementary Fig. 36 and Supplementary Video 3), indicating moisture absorption by the textile, which helps reduce surface dampness on the skin. Besides, we evaluated the moisture permeability and wicking properties of SilkNT (Fig. 3b, Supplementary Figs. 37–39 and Supplementary Video 4), revealing that they are comparable to those of commercial cotton and silk textiles. This can be attributed to the hydrophilicity nature of silk materials (see proof in Supplementary Figs. 40–42) and the unique hierarchical structures of the SilkNT.

The washability of textiles is a critical factor affecting their suitability for everyday use. To enhance the water-solubility resistance of SilkNT, we treated the SilkNT using ethanol to enhance the content of β-sheets in the regenerated silk nanofibre coating on the yarn surface. The treated SilkNT maintains its original optical properties (Supplementary Figs. 43–46) and micro-nano structure (Supplementary Fig. 47). After a single washing cycle (20 min in 40 °C water), the solar reflectance of the SilkNT is nearly unchanged (over 99% of its original value; Supplementary Figs. 48 and 49). Even after prolonged washing tests (5 h), the solar reflectance retains 95% of its initial value (Supplementary Fig. 49), while the infrared emittance shows no obvious change (Supplementary Fig. 50). The microstructures almost keep their pristine morphologies after washing (Supplementary Figs. 51 and 52), showing the excellent washability of the material.

Biocompatibility is of pivotal consideration for the practical application of textiles. In vitro studies using 3T3 cells as model cells have confirmed that SilkNT is non-cytotoxic. We compared the biocompatibility of SilkNT with conventional nanoparticle-enhanced textiles by coating aluminium oxide or titanium dioxide nanoparticles onto commercial silk textiles via partial surface dissolution (control groups) (Supplementary Fig. 53). Fluorescence images showed that the cells in the SilkNT sample exhibited regular morphology, with a notable increase in cell number with prolonged culture time, while the opposite trend was observed in the control group cells. In Cell Counting Kit-8 (CCK-8) assays, the absorbance at 450 nm (proportional to cell number) in the SilkNT group substantially differed from that in the control group. Absorbance at 450 nm in the SilkNT group increased with prolonged culture time, while absorbance in the control group decreased (Fig. 3c,d), indicating the excellent biocompatibility of SilkNT.

To assess the daytime cooling effect of SilkNT in a real-world scenario, we crafted a T-shirt by integrating a section of SilkNT into a commercially available silk T-shirt. We replaced a portion of the silk textile with the SilkNT patch to ensure the two parts (that is, SilkNT patch and silk T-shirt) had the same thickness. A volunteer wore the T-shirt and reclined under the sunlight for an hour, while thermocouples were placed under the T-shirt to monitor his skin temperature. The result reveals a temperature difference of approximately 4.3 °C between the two parts (Fig. 3e). In addition, thermal imaging was conducted when a volunteer wearing the SilkNT stood outdoors on a sunny day. Over a 10-min test, a remarkable temperature difference exceeding 1.3 °C was observed between the surfaces of the SilkNT (left) and the silk T-shirt (right) (Fig. 3f and Supplementary Fig. 54). SilkNT exhibits superior cooling performance compared with conventional textiles, effectively reducing the skin temperature. This enhanced cooling effect can be attributed to the unique interwoven silk nanofibre structure, which encapsulates the yarns in SilkNT. This design enables effective infrared emission through the atmospheric transparency window while also achieving high reflectivity in the visible and near-infrared ranges, thereby minimizing heat absorption from solar radiation.

We theoretically analysed the influence of the relative position between the person and buildings, and the reflectance of the ground and buildings on the radiative cooling performance of the SilkNT (Fig. 3g–i). We theoretically calculated ground temperature (T_{ground}) using common infrastructure materials, such as concrete (Supplementary Note 5). On a sunny day, the higher solar power and lower reflectance result in substantially elevated T_{ground} due to increased solar energy absorption (Fig. 3h). At a solar irradiance of 290 W m^{-2}, the T_{ground} reaches approximately 34 °C, approaching that of human skin (34 °C). On a sunny day in summer, when the solar irradiance reaches 800 W m^{-2}, the surface temperatures of the ground (52.4 °C) can easily exceed the average temperature of human skin. We employed a simplified model to calculate the radiative cooling power (P_{cool}) of vertically placed SilkNT in an open scenario surrounded by ground and buildings (Supplementary Note 6 and Supplementary Fig. 55). As shown in Fig. 3i, the high solar irradiance leads to deteriorated cooling performance. Assuming the textile temperature is equal to human skin temperature, when the solar irradiance is 290 W m^{-2} the textile temperature matches that of the surrounding ground or buildings. As a result, there is almost no heat exchange between them. However, the SilkNT continues to radiate energy to the cold outer space (around 2.7 K), and the net cooling power reaches 157.6 W m^{-2}. When the solar irradiance increases to 800 W m^{-2}, the surrounding ground and buildings become hotter than the SilkNT and the textile also absorbs heat radiation from them. Although the cooling effect is not as high as that under low solar irradiance, the P_{cool} of SilkNT (97.2 W m^{-2}) is still higher than the half of its initial value. These results indicate the potential of SilkNT for practical personal thermal management.

Sustainability of SilkNT

The SilkNT is biodegradable and recyclable. The SilkNT was subjected to the Pronase E solution at 37 °C. As a result, clear structural changes were observed in SilkNT after 10-day biodegradation, accompanied by

https://doi.org/10.1038/s41893-026-01887-8

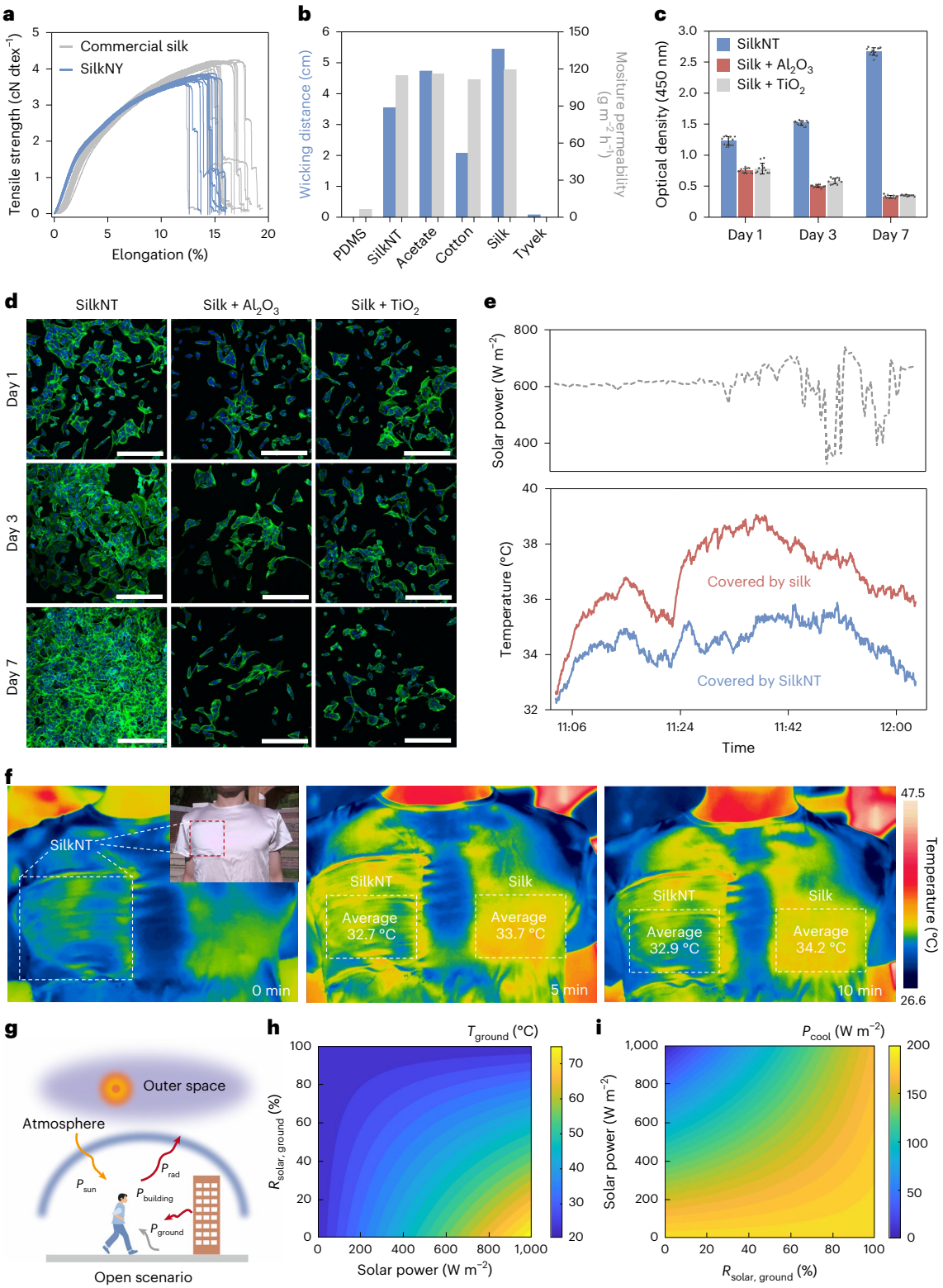


Fig. 3 | Mechanical properties, moisture permeability, wicking distance, biocompatibility and practical cooling performance of SilkNT. a, Mechanical strength of SilkNYs. **b**, Moisture permeability and wicking distance of different textiles. **c**, Absorption at 450 nm in a CCK-8 assay of different incubation groups after 1, 3 and 7 days of incubation. Data are presented as mean ± s.d. with individual data points overlaid. $n = 3$ independently seeded and treated wells per group. Each well was measured four times as technical replicates. The control group refers to cells cultured with nanoparticle-modified silk textiles. **d**, Fluorescence images of cells cultured in the incubation medium with the different groups. Scale bars, 300 µm. **e**, Temperature of the skin covered by different textiles (SilkNT and pristine silk) with direct sunlight radiation (Beijing, 12 September 2023). **f**, Infrared images of the volunteer with direct sunlight radiation, with all temperatures in degrees Celsius. **g**, A schematic showing a person standing in an open scenario surrounded by ground, sky and buildings. P_{rad}, radiative power. **h**, Theoretical ground temperature as a function of solar power and solar reflectance of ground ($R_{solar,ground}$). **i**, Simulated cooling power of vertically placed SilkNT under urban conditions. Positive values indicate net radiative cooling.

https://doi.org/10.1038/s41893-026-01887-8

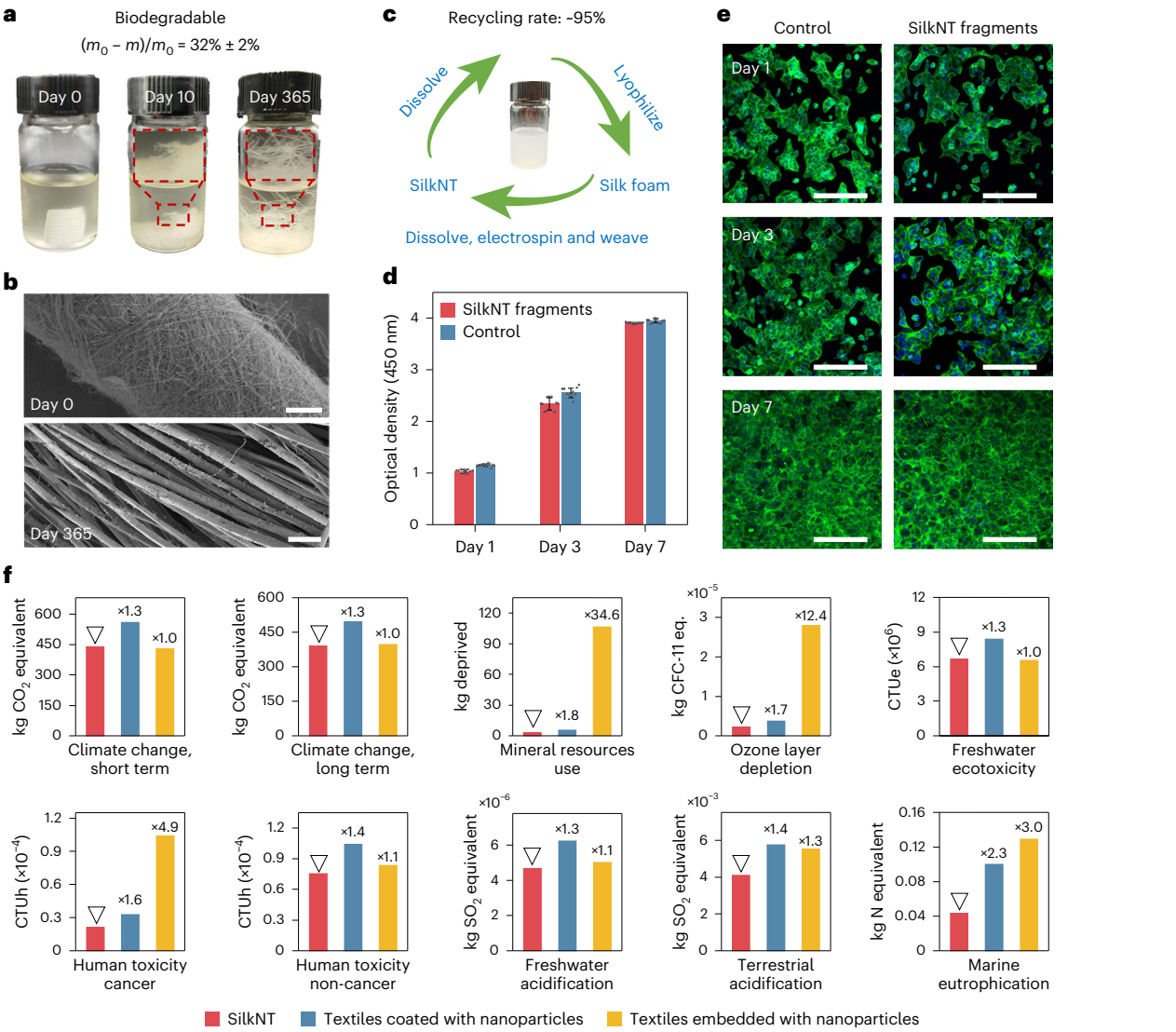


Fig. 4 | Biodegradability, recyclability and LCA of SilkNT, and biocompatibility of SilkNT fragments. a, Optical photographs showing the morphological changes of the SilkNT during the biodegradation test. m_0, the initial mass; m, mass after biodegradation. **b**, SEM images of SilkNY before biodegradation (day 0, top) and after 365 days of biodegradation (day 365, bottom). After 365 days of biodegradation, the sheath silk nanofibres have gone, with only the inner commercial silk yarn left. Scale bars, 50 µm. **c**, Demonstration of the recyclability of the SilkNT. **d**, Absorption at 450 nm in CCK-8 assay of different incubation groups after 1, 3 and 7 days of incubation. Data are presented as mean ± s.d. with individual data points overlaid. $n = 3$ independently seeded and treated wells per group. Each well was measured four times as technical replicates. The control group refers to cells cultured in blank medium without SilkNT fragments. **e**, Fluorescence images of cells cultured in the incubation medium. Scale bars, 300 µm. **f**, Comparison of impact categories with daytime radiative cooling textiles embedded or coated with toxic nanoparticles, referring to IMPACT World + Midpoint V1.03. CTUe, Comparative Toxic Unit for ecosystems, freshwater ecotoxicity; CTUh, Comparative Toxic Unit for humans, human toxicity; CFC-11, trichlorofluoromethane, the reference substance for ozone depletion.

the appearance of flocculus in the solution. After 365 days, the weight had decreased by 33% compared with its original weight (Fig. 4a). Morphological analysis revealed that majority of the regenerated silk nanofibres on the SilkNT surface have undergone biodegradation (Supplementary Fig. 56). The internal natural silk yarn also exhibited noticeable degradation after 365 days (Fig. 4b). To further corroborate the biodegradation process, infrared characterization was conducted on the flocculus generated after a 10 days of degradation (Supplementary Fig. 57). The spectra reveal a discernible weakening at the peaks corresponding to amide I (1,620 cm^{-1}) and amide II (1,520 cm^{-1}). The peak of amide III (1,230 cm^{-1}) vanishes, indicating a reduction in C=O and C–N stretching vibrations, characteristic of silk decomposition. The increase in the peak of amide IV (1,050 cm^{-1}) suggests an enhancement of (O=C–N) in-plane bending vibrations, signifying the transformation of regenerated silk from a long-chain peptide to a short-chain peptide, thus confirming the degradation of SilkNT. Besides, we observed that the SilkNT showed notable degradation in soil within 130 days, superior to other textiles made of PVDF-HFP, PE, polytetrafluoroethylene and nylon (Supplementary Fig. 58). Figure 4c illustrates that SilkNT is recyclable. During the recovery process, no additional separation treatments are required. The material can be easily recovered by employing the same treatment methods used for silk, yielding a recovery rate as high as 95% (Supplementary Fig. 59).

Given that SilkNT may produce micro- and nano-sized fibres or particles during degradation, we further evaluated the biosafety of micro- or nanometre-sized SilkNT fragments (Supplementary Figs. 60–62) with a cytotoxicity test. As shown in Fig. 4d, the result corresponding

to the SilkNT fragments group was nearly identical to that of the control group (blank medium), indicating excellent biocompatibility of SilkNT fragments. Fluorescence imaging revealed that the cell morphology in the SilkNT fragments group remained regular and the cell number substantially increased with extended incubation time, following the same trend observed in the control group (Fig. 4e).

An LCA was employed to assess the potential environmental impacts of SilkNT from aspects such as greenhouse gas emissions, resource consumption and human health. As depicted in Supplementary Fig. 63, cradle-to-grave is divided into three stages: textile preparation, use and end-of-life disposal. We conducted an LCA of two textile products from cradle to grave. For the control group, which required detailed preparation parameters, we referred to some detailed preparation parameters in previously reported daytime radiative cooling textiles with nanoparticles[5,19]. Detailed life cycle inventory and parameters are presented (Supplementary Note 7 and Supplementary Tables 3–15), including material and energy consumption during textile production, use and end-of-life disposal phases. The LCA results shown in Fig. 4f indicate that our SilkNT exhibits a lower environmental impact across the entire product life cycle compared with state-of-the-art daytime radiative cooling textiles with nanoparticles, especially with regard to human health. This can be ascribed to the absence of synthetic polymers and toxic nanoparticles in SilkNT, ensuring minimal environmental impact throughout its life cycle.

Discussion

SilkNT's key sustainability advantage stems from its monolithic, all-silk architecture, which achieves passive radiative cooling without addictives. This contrasts with most existing radiative cooling textiles that rely on incorporating of synthetic polymers and inorganic nanoparticles for optical management—a design that raises environmental concerns over microplastic pollution, nanoparticle release and end-of-life burdens. In SilkNT, silk functions simultaneously as the structural yarn and the nanoscale scattering medium, thereby retaining the necessary optical functions while eliminating exogenous polymers and engineered nanoparticles. This all-natural composition simplifies recycling, disposal and end-of-life treatment.

The cooling performance is enabled by multiscale structural engineering of silk. While natural silk fibres are too large to efficiently scatter sunlight, we process regenerated silk into nanofibres and helically wrap them around a silk core, creating a hierarchical, porous sheath. This nanostructured sheath boosts solar reflection through enhanced scattering and suppressed penetration, while the intrinsic molecular vibrations of silk provide high thermal emission in the atmospheric window. The design achieves function integration: the core provides mechanical robustness and wearability, while the nanofibre sheath delivers optical regulation, thus combining the optical functionality required for radiative cooling with the mechanical strength necessary for practical wearability within a single material system.

This structure-led, material-simplification principle demonstrated here is not limited to silk. It can guide the design of high-performance cooling materials from a wide range of natural and bio-based feedstocks. Beyond personal cooling textiles, such engineered bio-based architectures could be adapted to across multiple scales: from large-area building envelopes and temporary shelters, to mobile applications such as vehicle covers, and further to critical industries such as agricultural shade fabrics. In all these applications, efficient cooling and sustainable end-of-life outcomes are both critical. Accordingly, future sustainable cooling materials should be evaluated holistically across cooling power, durability, comfort, scalability and life-cycle impact. This study thus provides a generalizable design framework for developing high-performance thermal regulators from natural materials, reducing reliance on synthetic composites and their associated environmental and health burdens.

Methods

Materials

Formic acid (analytical reagent grade) was purchased from Macklin. *N*,*N*-Dimethylformamide (analytical reagent grade) was purchased from ADAMAS-BETA. Acetone (analytical reagent grade) was purchased from Tgreag. Silk yarns (145 g and 9,000 m) were purchased from Shengzhou Xiehe Silk Co. Silk textiles were purchased from Hangzhou Warren Textile Co. with a density of 129 g m^{-2}. The cotton textile (188 g m^{-2}) and acetate textile (215 g m^{-2}) were purchased from the local market. The aluminium oxide nanoparticles with diameters ranging from 150 to 500 nm and titanium dioxide nanoparticles with diameters ranging from 100 to 300 nm were purchased from Xfnano and Meryer, respectively. Poly(vinylidene fluoride-hexafluoropropylene) (average M_w ~455,000, average M_n ~110,000, pellets) was purchased from Sigma-Aldrich.

SilkNT preparation

Regenerated silk was prepared following the method in previous work[52]. To prepare the electrospinning solution, regenerated silk and formic acid were mixed in a mass ratio of 4:50 using a SpeedMixer (Flack Tek, Inc. DAC 150.1 FVZ-K) for 15 min at 3,000 rpm. The obtained solution was used for electrospinning nanofibres on the surface of the silk yarns. Electrospinning was conducted using two 23-gauge needle tips, with a positive voltage of 6 kV and a negative voltage of 8 kV. The feeding rate was 0.30 ml h^{-1} to 0.35 ml h^{-1}, and the bowl speed used to collect nanofibres onto the silk yarns was 250 rpm. The speed of the roller for collecting the yarn was 10 m h^{-1}. The silk yarn was positioned at the centre of the rotating bowl. Positively and negatively charged nanofibres were generated by electrostatic high voltage. One end of the nanofibres was attracted and fixed to the yarn by electrostatic forces, while the other end was fixed to the edge of the rotating bowl. As the bowl rotates, the nanofibres were uniformly wrapped around the yarn. The electrospinning solution of PVDF-HFP was composed of solutes and solvents in a mass ratio of 1:5 (aluminium oxide nanoparticles: PVDF-HFP of 25 wt%). The solvents consisted of acetone and *N*,*N*-dimethylformamide (mass ratio of 3:7). A positive voltage of 4 kV and a negative voltage of 5 kV were used. The feeding rate was 0.30 ml h^{-1}, and the bowl speed used to collect nanofibres onto the silk yarns was 250 rpm. The speed of the roller for collecting the yarn was 10 m h^{-1}. The environmental temperature and humidity during electrospinning were maintained at 25°C ± 2 °C and 35% ± 5%, respectively. Finally, the obtained SilkNYs were treated with ethanol vapour for 1 day in an airtight container and then immersed in ethanol for 1 min. The prepared SilkNTs were plain-weave constructed with warp and weft densities of 55 and 100 (dense), 33 and 101 (loose) yarns per inch by a household loom (QX304), respectively. The optical characterizations were conducted using dense SilkNT and the collected data were used for practical calculation. The loose SilkNT were used for cooling performance tests and wearability tests in comparison with commercial textiles.

Optical characterizations of regenerated silk and SilkNT

To measure the reflectance and transmittance of the obtained SilkNT and commercial textiles, a UV–visible-infrared spectrophotometer (UV3600 PLUS, Shimadzu) equipped with a diffuse integrating sphere model (ISR-1503F) was used. Solar reflectance measurements were conducted using a standard barium sulfate as the reference, providing high diffuse reflectance across the solar spectrum[51,53,54]. A Fourier-transform infrared spectrophotometer (VERTEX 80, Bruker) equipped with a gold integrating sphere was used to measure the reflectance and transmittance in the range of 2–25 µm. A standard gold reference was used owing to its stable and near-perfect reflectance in the infrared region[51,53,54]. The complex refractive index of the regenerated silk was measured using an RC2-XI (J. A. Woollam) and an IR-VASE MARK II (J. A. Woollam). Specifically, the regenerated silk was dissolved in formic acid (at a weight ratio of 4:50) and spun onto a Si

substrate (1 cm × 1 cm) at a speed of 2,000 rpm. The obtained sample was placed in the fuming cupboard for 12 h to make formic acid volatile completely and used for the final test. The infrared absorption of the SilkNT was carried out using a Fourier-transform infrared spectrophotometer (VERTEX 70, Bruker) with attenuated total reflection attachment. Optical photographs were captured using optical microscopy (Leica DM 2700 P). The samples used for the characterization in the tests are SilkNT, of which yarns are treated with ethanol unless otherwise stated.

Morphological characterizations

Scanning electron microscopy (SEM) images were captured by the ZEISS MERLIN Compact (15 kV). Samples were spurted a platinum layer with a thickness of 15 nm by the electro-coating machine (Leica, EM ACE600). X-ray computed microtomography images were captured by Xradia 510 Versa.

Thermal measurements of SilkNT

The real-time temperature was monitored with a homemade device. The measurements were carried out on the rooftop of the Department of Chemistry at Tsinghua University, Beijing (40°0′21.6″ N, 116°19′13.8″ E). In the subambient temperature cooling test, a piece of SilkNT with a size of 5 × 5 cm was placed on the groove of a polystyrene foam (20 × 20 cm) and stacked on the simulated skin. The simulated skin comprised a PDMS layer and a painting-coated copper plate with a polyimide heater (4 × 4 cm). To reduce thermal resistance between the heater and the copper plate, thermally conductive grease (Thermalright TF8) was used to fill the gap between them. Ambient and sample temperatures were monitored using K-type thermocouples (Kaipusen) linked to the data acquisition system (Meacon, MIK-R6000C). The ambient temperature was measured in a well-ventilated environment, specifically in a sun-shaded area with free air flow near the sample. The sample temperature was obtained from the average values reading on the two thermocouples. The wind speed and relative humidity were recorded by a commercial weather station (Shandong Renke Control Technology Co.). The outdoor test set up for commercial textiles was the same as that for the test of SilkNT. During the test, the simulated skin heater worked with a voltage of 1.71 V. All temperature data was acquired using the above data acquisition system. The solar power was recorded by a data-logging solar radiometer with an accuracy of ±5% (TES1333R, TES Electrical Electronic).

Washing test and wicking test

The washability of the SilkNT was tested using a standard washing fastness tester (Hengyu, HY-624A). The SilkNT was subjected to a single washing cycle for 20 min and an extended washing test for 5 h in 40 °C water with ECE Standard Detergent 98 (China Textile Standard Inspection and Certification Co.). The wicking testing procedure was based on AATCC TM 197 with modification. The textile samples were cut into 4-cm-wide strips and dipped into distilled water. We measured the climbing distance of the water in 30 min. The infrared camera was used for capturing the infrared images during the wicking process.

Wettability characterization

The wettability tests were performed using a Dataphysics OCA15Pro apparatus. SilkNT or cast silk films were affixed to a glass substrate using conductive adhesive (with a very flat surface) and placed on a carrier stage. The carrier stage was moved upward to bring the droplet (3 µl) to the tip of the needle by contacting with the SilkNT or the cast silk films. After contact, the stage was immediately moved downward to a certain position. The entire process was recorded using a high-speed video camera. Angle images were captured once the droplet stabilized on the SilkNT or the cast silk films. The angle was automatically generated by the software.

Investigation of the cell cytotoxicity

According to ISO 10993-5:2009 (E) standard, 3T3 cells (ATCC) were employed to assess the in vitro cytotoxicity of the SilkNT and SilkNT fragments. First, 5×10^4 3T3 cells in 1 ml full Dulbecco's modified Eagle medium (DMEM) were seeded in a 24-well plate and incubated for 24 h. After verifying cell confluence and morphology, the culture medium in the wells was discarded and 1 ml of fresh full medium was added. Then, 0.2 cm^2 sterile SilkNT and silk textiles with aluminium oxide and titanium dioxide nanoparticles (a dispersion of 30 wt% nanoparticles in formic acid was coated onto silk textiles and after being placed in a fume hood for 12 h, the obtained textiles were rinsed once in deionized water and dried) were directly added to the 24-well plates to allow sufficient contact with the medium to assess the cytotoxicity of the textiles. For the cytotoxicity test of SilkNT fragments: 2.5 g of SilkNT (cut into pieces) was added to 500 ml of deionized water and subjected to high-speed mechanical crushing (PHINIU, 2,600 W) for 2 h, followed by freeze-drying to obtain the SilkNT fragments. The resulting fragments were then suspended in a solution at a concentration of 10 mg ml^{-1}, sonicated for 5 min autoclaved for sterilization and subsequently diluted to 2.5 mg ml^{-1} with DMEM. Then, 1 ml of the prepared suspension was added to each well to assess the cytotoxicity of the SilkNT fragments. All samples were cultured in an incubator at 37 °C with 5% CO_2. After 1, 3 and 7 days of incubation, the cells were observed under a fluorescence microscope (Zeiss) and the CCK-8 assay was used to quantitatively detect cell proliferation. Each sample consisted of three parallel sets and each parallel set was measured four times.

Biodegradation and recyclability test of SilkNT

The SilkNT was immersed in a 0.01 M phosphate-buffered saline (PBS) solution at 37 °C with a concentration of 10 U ml^{-1} Pronase E (P8811, Sigma) for conducting biodegradation tests. The remaining mass of the SilkNT was measured at the end of the test, and SEM images were taken to observe its morphological changes. For the natural degradation experiment with SilkNT, we utilized 2.5 kg of commercially available planting soil, to which 500 g of EM composting bacteria (Captain Garden) were added and thoroughly mixed. Grass seeds were then sprinkled over the soil and different textiles were placed on the soil surface. The set up was watered every 2 days and the degradation process was recorded through regular photography. To assess the recyclability, the SilkNT (0.68 g) was treated following the method in previous work[52]. The results showed that the obtained regenerated silk could be used to create SilkNT again.

Reporting summary

Further information on research design is available in the Nature Portfolio Reporting Summary linked to this article.

Data availability

All data are available in this article and its Supplementary Information. Source data are provided with this paper.

References

1. *IPCC Special Report on Global Warming of 1.5 °C* (eds Masson-Delmotte, V. et al.) 3–24 (Cambridge Univ. Press, 2018).
2. Akram, H. M. A. et al. Textile recycling—a review. *Glob. J. Eng. Technol. Adv.* **6**, 069–074 (2021).
3. De Falco, F. et al. Evaluation of microplastic release caused by textile washing processes of synthetic fabrics. *Environ. Pollut.* **236**, 916–925 (2018).
4. De Falco, F. et al. Novel finishing treatments of polyamide fabrics by electrofluidodynamic process to reduce microplastic release during washings. *Polym. Degrad. Stab.* **165**, 110–116 (2019).
5. Zeng, S. N. et al. Hierarchical-morphology metafabric for scalable passive daytime radiative cooling. *Science* **373**, 692–696 (2021).

6. Yang, C. L. et al. Scalable fabrication of PVDF/SiO-PTFE fiber membrane for effective daytime radiative cooling. *Mater. Lett.* **320**, 132372 (2022).
7. Wu, X. E. et al. Durable radiative cooling multilayer silk textile with excellent comprehensive performance. *Adv. Funct. Mater.* **34**, 2313539 (2024).
8. Wu, X. et al. A dual-selective thermal emitter with enhanced subambient radiative cooling performance. *Nat. Commun.* **15**, 815 (2024).
9. Song, Y. N., Lei, M. Q., Lei, J. & Li, Z. M. Spectrally selective polyvinylidene fluoride textile for passive human body cooling. *Mater. Today Energy* **18**, 100504 (2020).
10. Cheng, N. et al. Nanosphere-structured hierarchically porous PVDF-HFP fabric for passive daytime radiative cooling via one-step water vapor-induced phase separation. *Chem. Eng. J.* **460**, 141581 (2023).
11. Li, D. et al. Scalable and hierarchically designed polymer film as a selective thermal emitter for high-performance all-day radiative cooling. *Nat. Nanotechnol.* **16**, 153–158 (2021).
12. Yao, P. et al. Spider-silk-inspired nanocomposite polymers for durable daytime radiative cooling. *Adv. Mater.* **34**, e2208236 (2022).
13. Wu, X. K. et al. An all-weather radiative human body cooling textile. *Nat. Sustain.* **6**, 1446–1454 (2023).
14. Fan, C. et al. Dynamically tunable subambient daytime radiative cooling metafabric with Janus wettability. *Adv. Funct. Mater.* **33**, 230079 (2023).
15. Miao, D., Cheng, N., Wang, X., Yu, J. & Ding, B. Integration of Janus wettability and heat conduction in hierarchically designed textiles for all-day personal radiative cooling. *Nano Lett.* **22**, 680–687 (2022).
16. Cai, X., Gao, L., Wang, J. & Li, D. MOF-integrated hierarchical composite fiber for efficient daytime radiative cooling and antibacterial protective textiles. *ACS Appl. Mater. Interfaces* **15**, 8537–8545 (2023).
17. Zhong, S. J. et al. Self-cleaning and spectrally selective coating on cotton fabric for passive daytime radiative cooling. *Chem. Eng. J.* **407**, 127104 (2021).
18. Peng, Y. et al. Nanoporous polyethylene microfibres for large-scale radiative cooling fabric. *Nat. Sustain.* **1**, 105–112 (2018).
19. Zhu, B. et al. Subambient daytime radiative cooling textile based on nanoprocessed silk. *Nat. Nanotechnol.* **16**, 1342–1348 (2021).
20. Cai, L. et al. Spectrally selective nanocomposite textile for outdoor personal cooling. *Adv. Mater.* **30**, 1802152 (2018).
21. Boucher, J. & Friot, D. *Primary Microplastics in the Oceans: A Global Evaluation of Sources* (IUCN, 2017).
22. Lahiri, S. K., Dijvejin, Z. A. & Golovin, K. Polydimethylsiloxane-coated textiles with minimized microplastic pollution. *Nat. Sustain.* **6**, 559–567 (2023).
23. Brahney, J., Hallerud, M., Heim, E., Hahnenberger, M. & Sukumaran, S. Plastic rain in protected areas of the United States. *Science* **368**, 1257–1260 (2020).
24. Evangeliou, N. et al. Atmospheric transport is a major pathway of microplastics to remote regions. *Nat. Commun.* **11**, 3381 (2020).
25. Bergmann, M. et al. White and wonderful microplastics prevail in snow from the Alps to the Arctic. *Sci. Adv.* **5**, eaax1157 (2019).
26. Jeng, H. A. & Swanson, J. Toxicity of metal oxide nanoparticles in mammalian cells. *J. Environ. Sci. Health A* **41**, 2699–2711 (2006).
27. Wang, Y. et al. In vivo degradation of three-dimensional silk fibroin scaffolds. *Biomaterials* **29**, 3415–3428 (2008).
28. Horan, R. L. et al. In vitro degradation of silk fibroin. *Biomaterials* **26**, 3385–3393 (2005).
29. Bergman, T. L., Lavine, A. S., Incropera, F. P. & DeWitt, D. P. *Fundamentals of Heat and Mass Transfer* 6th edn, Vol. 6 (Wiley, 2018).
30. Shi, N. N. et al. Nanostructured fibers as a versatile photonic platform: radiative cooling and waveguiding through transverse Anderson localization. *Light: Sci. Appl.* **7**, 37 (2018).
31. Zhang, Y. et al. Atmospheric water harvesting by large-scale radiative cooling cellulose-based fabric. *Nano Lett.* **22**, 2618–2626 (2022).
32. Ahmed, A. T. M. F., Islam, M. Z., Mahmud, M. S., Sarker, M. E. & Islam, M. R. Hemp as a potential raw material toward a sustainable world: a review. *Heliyon* **8**, e08753 (2022).
33. Bodurov, I., Vlaeva, I., Viraneva, A., Yovcheva, T. & Sainov, S. Modified design of a laser refractometer. *Nanosci. Nanotechnol.* **16**, 31–33 (2016).
34. Sultanova, N., Kasarova, S. & Nikolov, I. Dispersion properties of optical polymers. *Acta Phys. Pol. A* **116**, 585–587 (2009).
35. Mie, G. Beiträge zur optik trüber medien, speziell kolloidaler metallösungen. *Ann. Phys.* **330**, 377–445 (1908).
36. Wang, X. et al. Scalable flexible hybrid membranes with photonic structures for daytime radiative cooling. *Adv. Funct. Mater.* **30**, 1907562 (2019).
37. He, J. et al. Scalable nanofibrous silk fibroin textile with excellent Mie scattering and high sweat evaporation ability for highly efficient passive personal thermal management. *Chem. Eng. J.* **466**, 143127 (2023).
38. Li, J. et al. Protecting ice from melting under sunlight via radiative cooling. *Sci. Adv.* **8**, eabj9756 (2022).
39. Zhang, D. et al. Abrasion resistant/waterproof stretchable triboelectric yarns based on Fermat spirals. *Adv. Mater.* **33**, e2100782 (2021).
40. Kirchhoff, G. Ueber das verhältniss zwischen dem emissionsvermögen und dem absorptionsvermögen der körper für wärme und licht. *Ann. Phys.* **185**, 275–301 (1860).
41. Xue, X. et al. Creating an eco-friendly building coating with smart subambient radiative cooling. *Adv. Mater.* **32**, e1906751 (2020).
42. Wang, X. et al. Sub-ambient full-color passive radiative cooling under sunlight based on efficient quantum-dot photoluminescence. *Sci. Bull.* **67**, 1874–1881 (2022).
43. Mandal, J. et al. Hierarchically porous polymer coatings for highly efficient passive daytime radiative cooling. *Science* **362**, 315–319 (2018).
44. Chen, Y. et al. Colored and paintable bilayer coatings with high solar-infrared reflectance for efficient cooling. *Sci. Adv.* **6**, eaaz5413 (2020).
45. Mandal, J., Yang, Y., Yu, N. & Raman, A. P. Paints as a scalable and effective radiative cooling technology for buildings. *Joule* **4**, 1350–1356 (2020).
46. Mandal, J. et al. Porous polymers with switchable optical transmittance for optical and thermal regulation. *Joule* **3**, 3088–3099 (2019).
47. Cheng, Q. et al. Cost-effective bilayer radiative cooling paint via a porous P(VDF-HFP) top layer. *Adv. Funct. Mater.* **35**, 2506405 (2025).
48. Chen, Y. et al. Personal microenvironment management by smart textiles with negative oxygen ions releasing and radiative cooling performance. *ACS Nano* **17**, 13269–13277 (2023).
49. Li, K. et al. A Janus textile capable of radiative subambient cooling and warming for multi-scenario personal thermal management. *Small* **19**, e2206149 (2023).
50. Yan, Z., Zhai, H., Fan, D. & Li, Q. A trimode textile designed with hierarchical core-shell nanofiber structure for all-weather radiative personal thermal management. *Nano Today* **51**, 101897 (2023).
51. Zhang, Q. et al. Daytime radiative cooling dressings for accelerating wound healing under sunlight. *Nat. Chem. Eng.* **1**, 301–310 (2024).

52. Rockwood, D. N. et al. Materials fabrication from *Bombyx mori* silk fibroin. *Nat. Protoc.* **6**, 1612–1631 (2011).
53. Wu, R. et al. Spectrally engineered textile for radiative cooling against urban heat islands. *Science* **384**, 1203–1212 (2024).
54. Li, J. et al. A photosynthetically active radiative cooling film. *Nat. Sustain.* **7**, 786–795 (2024).

Acknowledgements

We thank X. Wang from the Department of Chemical Engineering, Tsinghua University, for her valuable guidance and assistance in the life cycle assessment.

Author contributions

Yingying Zhang and W.C. supervised the project. X.-E.W. and Yingying Zhang conceived of the idea. X.-E.W. and Y.W. designed the experiments and performed the material preparation and characterization with the help of Yong Zhang, H. Lu, L.Z., M. Jiang, M. Zhu, M. Zou, H. Liang, Yaoyao Zhou, P.B. and X.L. S.L. participated in the heat transfer analysis. M. Jian participated in the washing test of the SilkNT. R.Y. and L.Z. participated in the cell cytotoxicity test. X.-E.W., Y.W., Yingying Zhang and W.C. co-wrote the paper with input from all the authors.

Funding

Yingying Zhang discloses support for the research of this work from the National Natural Science Foundation of China (grant no. 52125201) and National Key Basic Research and Development Program (grant no. 2024YFA0919304). Y.W. discloses support for publication of this work from the China Postdoctoral Science Foundation (grant no. 2023M731868).

Competing interests

The authors declare no competing interests.

Additional information

Supplementary information The online version contains supplementary material available at https://doi.org/10.1038/s41893-026-01887-8.

Correspondence and requests for materials should be addressed to Wenshuai Chen or Yingying Zhang.

Peer review information *Nature Sustainability* thanks Kevin Golovin, Po-Chun Hsu, Ronghui Wu and the other, anonymous, reviewer(s) for their contribution to the peer review of this work.

Reprints and permissions information is available at www.nature.com/reprints.

Publisher's note Springer Nature remains neutral with regard to jurisdictional claims in published maps and institutional affiliations.

Springer Nature or its licensor (e.g. a society or other partner) holds exclusive rights to this article under a publishing agreement with the author(s) or other rightsholder(s); author self-archiving of the accepted manuscript version of this article is solely governed by the terms of such publishing agreement and applicable law.

© The Author(s), under exclusive licence to Springer Nature Limited 2026

nature portfolio

Corresponding author(s): Yingying Zhang, Wenshuai Chen

Last updated by author(s): May 8, 2026

Reporting Summary

Nature Portfolio wishes to improve the reproducibility of the work that we publish. This form provides structure for consistency and transparency in reporting. For further information on Nature Portfolio policies, see our Editorial Policies and the Editorial Policy Checklist.

Statistics

For all statistical analyses, confirm that the following items are present in the figure legend, table legend, main text, or Methods section.

n/a	Confirmed	
☐	☒	The exact sample size (*n*) for each experimental group/condition, given as a discrete number and unit of measurement
☐	☒	A statement on whether measurements were taken from distinct samples or whether the same sample was measured repeatedly
☒	☐	The statistical test(s) used AND whether they are one- or two-sided *Only common tests should be described solely by name; describe more complex techniques in the Methods section.*
☒	☐	A description of all covariates tested
☒	☐	A description of any assumptions or corrections, such as tests of normality and adjustment for multiple comparisons
☐	☒	A full description of the statistical parameters including central tendency (e.g. means) or other basic estimates (e.g. regression coefficient) AND variation (e.g. standard deviation) or associated estimates of uncertainty (e.g. confidence intervals)
☒	☐	For null hypothesis testing, the test statistic (e.g. *F*, *t*, *r*) with confidence intervals, effect sizes, degrees of freedom and *P* value noted *Give P values as exact values whenever suitable.*
☒	☐	For Bayesian analysis, information on the choice of priors and Markov chain Monte Carlo settings
☒	☐	For hierarchical and complex designs, identification of the appropriate level for tests and full reporting of outcomes
☒	☐	Estimates of effect sizes (e.g. Cohen's *d*, Pearson's *r*), indicating how they were calculated

Our web collection on statistics for biologists contains articles on many of the points above.

Software and code

Policy information about availability of computer code

Data collection	FLIR Tools, Microscope imaging software from Leica Microsystems, Meacon-MIK-R6000C
Data analysis	Origin 2018, Matlab R2021a, SimaPro 9.5

For manuscripts utilizing custom algorithms or software that are central to the research but not yet described in published literature, software must be made available to editors and reviewers. We strongly encourage code deposition in a community repository (e.g. GitHub). See the Nature Portfolio guidelines for submitting code & software for further information.

Data

Policy information about availability of data

All manuscripts must include a data availability statement. This statement should provide the following information, where applicable:

- Accession codes, unique identifiers, or web links for publicly available datasets
- A description of any restrictions on data availability
- For clinical datasets or third party data, please ensure that the statement adheres to our policy

All data generated or analysed in this study are included in this published article (and its supplementary information files).

Research involving human participants, their data, or biological material

Policy information about studies with human participants or human data. See also policy information about sex, gender (identity/presentation), and sexual orientation and race, ethnicity and racism.

Reporting on sex and gender	One male volunteer was involved in the wearing temperature monitoring experiments.
Reporting on race, ethnicity, or other socially relevant groupings	The volunteer is from eastern Asia.
Population characteristics	The volunteer is male and is healthy, with no allergies. The age of volunteer is 27.
Recruitment	Volunteer was invited by open recruitment in Department of Chemistry, Tsinghua University, to participate this research. Volunteer was required to be healthy and had no allergies.
Ethics oversight	The data was obtained with the informed consent of the participant. The Institutional Review Board of Tsinghua University (No. 20230019) approved this study.

Note that full information on the approval of the study protocol must also be provided in the manuscript.

Field-specific reporting

Please select the one below that is the best fit for your research. If you are not sure, read the appropriate sections before making your selection.

☐ Life sciences ☐ Behavioural & social sciences ☒ Ecological, evolutionary & environmental sciences

For a reference copy of the document with all sections, see nature.com/documents/nr-reporting-summary-flat.pdf

Ecological, evolutionary & environmental sciences study design

All studies must disclose on these points even when the disclosure is negative.

Study description	We attached some thermocouples on the skin of the volunteer. Then we put our hand-made T-shirt with different textiles covered regions on the volunteer. We let him standing outside to monitor the temperature change during the test. In addition, we used IR camera to collect IR images of the subject during the test. All the data we collected is to prove our all-silk textile have better cooling performance than the commercial textiles.
Research sample	We selected a healthy male adult with no allergies to participate in the wearing temperature monitoring experiments.
Sampling strategy	We conducted the wearing temperature monitoring experiments in outdoor condition for one time.
Data collection	12 September 2023
Timing and spatial scale	One hour at the same location.
Data exclusions	No data exclusion involved.
Reproducibility	No reproducibility was need. We analyzed all date tested in the same time period and location to show our all-silk textile covered area has better cooling performance than that covered by the commercial textiles.
Randomization	No randomization was used. We analyzed all the results of the test.
Blinding	No blinding is necessary since we analyzed all the temperature data collected with the help of the volunteer.

Did the study involve field work? ☒ Yes ☐ No

Field work, collection and transport

Field conditions	The experiment was conducted in a sunny day. The outdoor temperature was monitored during the test, and was around 30 degrees Celsius.
Location	At the square in front of the building of Department of Chemistry, Tsinghua University.
Access & import/export	N/A

Disturbance	N/A

Reporting for specific materials, systems and methods

We require information from authors about some types of materials, experimental systems and methods used in many studies. Here, indicate whether each material, system or method listed is relevant to your study. If you are not sure if a list item applies to your research, read the appropriate section before selecting a response.

Materials & experimental systems

n/a	Involved in the study
☒	☐ Antibodies
☐	☒ Eukaryotic cell lines
☒	☐ Palaeontology and archaeology
☒	☐ Animals and other organisms
☒	☐ Clinical data
☒	☐ Dual use research of concern
☒	☐ Plants

Methods

n/a	Involved in the study
☒	☐ ChIP-seq
☒	☐ Flow cytometry
☒	☐ MRI-based neuroimaging

Eukaryotic cell lines

Policy information about cell lines and Sex and Gender in Research

Cell line source(s)	The cell line NIH/3T3 was obtained from Wuhan Servicebio Technology Co., Ltd
Authentication	All cell lines were authenticated using STR analysis according toto the ICLAC guidelines.
Mycoplasma contamination	All cell lines were routinely tested for mycoplasma and tested negative.
Commonly misidentified lines (See ICLAC register)	No commonly misidentified cell lines were used in this study.

Plants

Seed stocks	N/A
Novel plant genotypes	N/A
Authentication	N/A